

# Using Wavelet-Based Functional Mixed Models to Characterize Population Heterogeneity in Accelerometer Profiles: A Case Study

Jeffrey S. Morris<sup>1</sup>, Cassandra Arroyo<sup>2</sup>, Brent Coull<sup>3</sup>,  
Louise M. Ryan<sup>3,4</sup>, Richard Herrick<sup>1</sup>, and Steven L. Gortmaker<sup>5</sup>

<sup>1</sup>Department of Biostatistics and Applied Mathematics,

The University of Texas M.D. Anderson Cancer Center, Houston, TX

<sup>2</sup>Social Epidemiology Research Center, Morehouse School of Medicine, Atlanta, GA

<sup>3</sup>Department of Biostatistics, Harvard School of Public Health, Boston, MA

<sup>4</sup>Dana-Farber Cancer Institute, Boston, MA

<sup>5</sup>Department of Society, Human Development, and Health, Harvard School of Public Health, Boston, MA

January 5, 2005

## SUMMARY

We present a case study illustrating the challenges of analyzing accelerometer data taken from a sample of children participating in an intervention study designed to increase physical activity. An accelerometer is a small device worn on the hip that records the minute-by-minute activity levels of the child throughout the day for each day it is worn. The resulting data are irregular functions characterized by many peaks representing short bursts of intense activity. We model these data using the wavelet-based functional mixed model. This approach incorporates multiple fixed effect and random effect functions of arbitrary form, the estimates of which are adaptively regularized using wavelet shrinkage. The method yields posterior samples for all functional quantities of the model, which can be used to perform various types of Bayesian inference and prediction. In our case study, a high proportion of the daily activity profiles are incomplete, i.e. have some portion of the profile missing, so cannot be directly modeled using the previously described method. We present a new method for stochastically imputing the missing data that allows us to incorporate these incomplete profiles in our analysis. Our approach borrows strength from both the observed measurements within the incomplete profiles and from other profiles, from the same child as well as other children with similar covariate levels, while appropriately propagating the uncertainty of the imputation throughout all subsequent inference. We apply this method to our case study, revealing some interesting insights into children's activity patterns. We point out some strengths and limitations of using this approach to analyze accelerometer data.

*Keywords: Accelerometer, Bayesian inference, functional data analysis, missing data, mixed models, wavelets, wavelet regression.*

Short Title: Modeling Accelerometer Data Using Functional Mixed Models

# 1 Introduction

Physical activity during childhood and adolescence has an impact on a number of different aspects of subsequent health and well-being. Studies have suggested that increased physical activity during the childhood and adolescent years can (1) help build and maintain healthy bones, muscles and joints; (2) help control weight, build lean muscles and reduce fat; (3) prevent or delay the development of hypertension, and help reduce blood pressure in some adolescents with hypertension; (4) reduce feelings of depression and anxiety; (5) positively influence mental health and feelings of independence; and (6) positively influence the development of self-esteem (CDC, 2000; CDC, 2001; Dietz 1998; Pearce, 1999; Strauss et al., 2001).

The systematic study of physical activity is complicated by the technical challenges of measurement. One common approach is to use self-report questionnaires, but these are known to correlate poorly with actual activity levels, often overestimating them (Matthews and Freedson 1995, Epstein et al. 1996, Coleman et al. 1997). Recently, more objective approaches have been used, including computerized accelerometers: small motion sensors that can digitally record minute-by-minute activity levels. Their small size and automatic measurement capabilities make them well-suited for objectively quantifying activity levels in large populations over long periods of time (Westerterp, 1999). They are being used increasingly to monitor activity levels in large surveillance studies and intervention trials, in children as well as adults (Rowlands, Eston, and Ingledew 1999; Rowlands et al. 2000; Gortmaker 2002; Going et al. 2003; Talbot et al. 2003; Algase et al. 2003; Abbott and Davies 2004). In this paper, we consider accelerometer data obtained from Planet Health (Gortmaker et al. 1999), a Boston-area study of a school-based intervention designed to reduce obesity in middle school youth by changing key physical activity and dietary risk factors.

The Planet Health study used the TriTrac-R3D activity monitor (Hemokentics, Inc., Madison, WI), which is worn in a small pouch on the hip and provides minute-by-minute acceleration counts computed from motion sensors in three-dimensional space. The resulting daily profiles are irregular functional data characterized by many peaks representing short bursts of intense

activity. Figure 1 contains two daily profiles from 9am to 8pm from two different children in the Planet Health study. Other accelerometers yield similar data. In studies involving accelerometers, it is standard practice to obtain 4 to 8 daily profiles for each subject in the study. These profiles can be analyzed directly, or used to calibrate and validate questionnaire-based measures of physical activity. In practice, many of the profiles are incomplete, having periods of time for which the activity levels are missing, for example, if the accelerometer is removed.

Approaches currently used to analyze these data are based on simple summaries, such as the average daily activity level (Talbot et al. 2003), 30-minute averages (Going et al. 2003; Craddock et al. 2004), or the proportion of time spent above specific cutoff levels that correspond to sedentary, moderately vigorous, and vigorous activity (Rowlands, Eston and Ingledew 1999; Goldfield et al. 2000; Westerterp 2001; Abbott and Davies 2004). While these summaries are a reasonable starting point, they have serious limitations, mostly because they do not make full use of the rich information contained in the functional data. The proportions and daily averages do not account for time of the day variability, and the proportions do not even use the actual activity levels. The arbitrary binning inherent to taking 30-minute averages results in attenuation of the signal, and conclusions may be sensitive to the choice of endpoints for the bins. A second important limitation of these approaches is that they may not effectively handle the missing data in the incomplete profiles, which is a serious concern considering the large degree of missingness that can occur in these data.

Methods that model the functional profiles in their entirety have the potential to extract more information from the data compared with methods based on arbitrarily chosen summary measures. For example, these methods are able to identify at what time of day children are most active, detect covariate effects that vary throughout different times of the day, and allow the variability in activity levels to differ across time of day. Functional data analysis (FDA, Ramsay and Silverman 1997) is a general name for approaches that consider the functional profiles as single entities rather than simply a collection of individual data points. A key challenge with these approaches is that they must deal both with regularization, or borrowing strength across

measurements within a profile, and replication, or combining information across multiple profiles to make inferences on the population from which they came.

The irregularity of accelerometer profiles makes them especially challenging to model in this manner. They clearly cannot be represented by simple parametric structures, and the most commonly-used nonparametric methods involve smoothing by kernels or splines, which are not well-suited for modeling functional data with many local features like peaks. Since there are typically multiple daily profiles per child, one must account for the possibility of correlation between profiles. Also, there are many factors potentially affecting the profiles, including the day of the week, time of year, school, and child-level characteristics like gender, age, and obesity status. The effects of these factors may vary by time of day. A suitable modeling approach should be able to simultaneously account for functional effects of multiple covariates like these, some of which are of interest to investigators, and others of which are potential confounders.

Morris and Carroll (2004) introduced a new method for analyzing functional data that accommodates these concerns. It is based on the functional mixed model, which is a generalization of the linear mixed model (Laird and Ware 1982) to functional data. The method is appropriate for modeling irregular profiles with many peaks, since regularization is accomplished using adaptive methods based on wavelet shrinkage. The functional mixed model allows multiple fixed effect functions of arbitrary form, which can simultaneously represent time-varying effects for multiple covariates, discrete or continuous in nature. It also allows multiple random effect functions of arbitrary form, which can model the correlation between profiles from the same child. The reasonably flexible assumptions made on the covariance matrices for the random effects and residual errors accommodate a broad range of nonstationary covariance structures. The output of the method consists of posterior samples for all quantities in the model, which can be used to perform Bayesian inference.

While the method of Morris and Carroll (2004) cannot handle incomplete profiles, it is based on a unified modeling approach, making it possible to develop rigorous methods for imputing the missing data. In this paper, we introduce new missing data methods for the wavelet-based

functional mixed model. Briefly, our approach is to stochastically sample the missing regions of the incomplete profiles from their approximate posterior predictive distributions, as estimated from a preliminary model fit using only the complete daily profiles. This approach results in a procedure that borrows strength both from the observed measurements within the incomplete profile and from other profiles, from the same child as well as other children with similar covariate levels. The method appropriately propagates the uncertainty due to the imputation throughout any subsequent inference.

We apply these methods to analyze the TriTrac-R3D data from the Planet Health study in order to explore patterns in the children’s activity level profiles, to identify factors related to activity levels, and to characterize the relative contributions of the day-to-day and child-to-child sources of variability in order to aid the design of future studies. We also assess the model fit, and discuss the strengths and limitations of this approach for analyzing accelerometer data.

The remainder of the paper is organized as follows. In Section 2, we describe the Planet Health study, and explore the characteristics of the TriTrac-R3D accelerometer data from that study. In Section 3, we give a brief overview of wavelets and the wavelet-based functional mixed model, and in Section 4, we introduce new methods for imputing missing data for incomplete profiles in the wavelet-based functional mixed models setting. In Section 5, we present the results of our case study analysis. Section 6 contains a discussion of these results and a general discussion of the strengths and limitations of this approach for analyzing accelerometer data. A technical appendix contains the derivation of the posterior predictive distributions used to impute the missing data.

## **2 Accelerometer Data from the Planet Health Study**

Childhood obesity is a major health problem in the United States. Planet Health was a school-based intervention designed to reduce obesity in middle school youth (grades 6-8) by changing key physical activity and dietary risk factors. The Planet Health study (Gortmaker et al. 1999) involved 10 Boston-area middle schools, which were paired up and randomized to either receive

the intervention or serve as control schools. For each of the 1295 children involved in the study, various nutritional, behavioral, and health-related outcomes were measured at baseline (fall 1995) and follow-up (spring 1997). A subsample of 256 children was randomly selected to participate in a substudy focusing on the technical issue of objectively measuring physical activity using accelerometers. The activity levels of each child in the substudy were monitored using the TriTrac-R3D activity monitor for one or two four-day sessions between February and May of 1997.

The TriTrac-R3D activity monitor is a pocket-sized motion sensor that, when worn on the hip in a nylon pouch, measures motion in three planes (horizontal, vertical, and mediolateral). The TriTrac stores data over a several days, after which the data can be downloaded to a computer to provide a minute-by-minute record of movement in each dimension. The counts in the three planes may be combined into a single activity level for each minute by computing the vector magnitude. The vector magnitudes may then be converted into estimated energy expenditure per minute due to activity (EE). The TriTrac-R3D uses a proprietary formula involving the subjects weight to compute EE; Gortmaker (2002) calculated this formula, and then converted these into METS (metabolic units) using  $MET = (EE + BMR) / BMR$ , where BMR is the child's basal metabolic rate, estimated from their gender, age, and weight using the World Health Organization (WHO) equations (*Recommended Daily Allowances* 2000). The minimum activity level is 1 MET, which indicates the child is stationary, while activities yielding levels between 3 and 6 MET (e.g., walking) are considered moderately intense, and activities yielding levels of more than 6 MET (e.g., running) are considered vigorous (Rowlands et al. 2004).

We focused on the weekday accelerometer profiles from children in the 5 control schools that did not receive the intervention. This data set consisted of 550 daily profiles from 112 children. Each daily profile contained 1440 measurements, the minute-by-minute activity levels for a single day, measured in METs. If no movement was recorded for 30 or more consecutive minutes, we assumed that the child removed the monitor, and the corresponding measurements were considered missing. Figure 2 contains a heatmap of the 550 daily profiles. A heatmap is a

graphical device that is useful for representing high-dimensional data sets. Each row corresponds to a single profile and each column is one minute in the day. The color of the pixel  $(i, j)$  indicates the activity level of profile  $i$  at time  $t_j$ , with higher activity levels represented by lighter colors. For this graph, we coded missing measurements as 0 (black), and censored moderate and vigorous activity levels ( $> 3.0$  MET, white) to improve the contrast of the figure. The white dashed horizontal lines delineate the schools, which we will refer to as schools A, B, C, D, and E, respectively. Note the imbalance in the number of profiles obtained from each school.

There were a large number of missing measurements in the data. Figure 3(a) contains a plot of the proportion of daily profiles with nonmissing measurements as a function of the time of the day. We focused our analysis on the data from 9am to 8pm, since most of the profiles were missing outside this region. Figure 3(b) contains a histogram of the proportion of minutes missing from 9am-8pm for the 550 profiles. Only 95 of the 550 profiles were complete from 9am to 8pm, and 187 profiles had more than 80% of this region missing. We focused on the 292 profiles that were at least 50% complete from 9am to 8pm, which were from 106 children. All of these profiles were obtained between February 10, 1997 and May 28, 1997.

For each child, we had a number of covariate measurements, including their school, race, gender, age, weight, height, body mass index (BMI), triceps skinfold (measured by skinfold calipers applied to the triceps), and average number of hours spent watching television per day. We also had a record of the day-of-week and the calendar date on which each profile was obtained.

We were interested in assessing how activity levels tended to vary throughout the day, across schools, across different days of the week, over time from early to late spring, and across various child-level covariates. We also were interested in assessing the relative variability from day to day and child to child, in order to provide design recommendations for future studies. We accomplished these goals by applying the wavelet-based functional mixed model to these data, after adapting the procedure to accomodate incomplete profiles. We assessed how well this model fit the data, and specifically checked how closely it predicted the frequency of bouts of

moderate and vigorous activity for groups of children as a function of the time of day.

### 3 Wavelets and Functional Mixed Models

#### 3.1 Brief Review of Wavelets

Wavelets are basis functions that can be used to represent other functions, often very parsimoniously. Basic introductions to wavelets can be found in Burrus, Gopinath and Guo (1998) and Goswami and Chan (1999). A wavelet series approximation to a continuous function  $y(t)$  is given by

$$y(t) = \sum_k c_{J,k} \phi_{J,k}(t) + \sum_{j=1}^J \sum_k d_{j,k} \psi_{j,k}(t), \quad (1)$$

where  $J$  is the number of scales, and  $k$  ranges from 1 to the  $K_j$ , the number of coefficients at scale  $j$ . The functions  $\phi_{J,k}(t)$  and  $\psi_{j,k}(t)$  are wavelet basis functions, which are dilations and translations of a father and mother wavelet function,  $\phi(t)$  and  $\psi(t)$ , respectively, with  $\phi_{j,k}(t) = 2^{-j/2} \phi(2^{-j}t - k)$  and  $\psi_{j,k}(t) = 2^{-j/2} \psi(2^{-j}t - k)$ .

The coefficients  $c_{J,k}, d_{J,k}, \dots, d_{1,k}$  are the *wavelet coefficients*. The  $c_{J,k}$  are called the *smooth* coefficients, and represent smooth behavior of the function at coarse scale  $J$ , and the  $d_{j,k}$  are called the *detail* coefficients, and represent deviations of the function at scale  $j$ , where smaller  $j$  correspond to finer scales. Theoretically, each coefficient may be obtained by taking the inner product of the function and the corresponding wavelet basis function, although in practice more efficient approaches are typically used. If the function is sampled on an equally spaced grid of length  $T$ , then the coefficients may be computed using a pyramid-based algorithm called the discrete wavelet transform (DWT) in just  $O(T)$  operations. Applying the DWT to a row vector of observations  $\mathbf{y}$  produces a row vector of wavelet coefficients  $\mathbf{d} = (c_{J,1}, \dots, c_{J,K_J}, d_{J,1}, \dots, d_{1,K_1})$ . This transformation is a linear projection, so it may also be represented by matrix multiplication,  $\mathbf{d} = \mathbf{y}W'$ , with  $W'$  being the DWT projection matrix. Similarly, the inverse discrete wavelet transform (IDWT) may be used to project wavelet coefficients back into the data space, and can also be represented by matrix multiplication by the IDWT projection matrix  $W$ , which is the transpose of the DWT projection matrix.

Wavelets may be used to perform nonparametric regression using the following three-step procedure. First, noisy data  $\mathbf{y}$  are projected into the wavelet domain using the DWT, yielding empirical wavelet coefficients  $\mathbf{d}$ . The coefficients are then thresholded by setting to zero any coefficients smaller in magnitude than a specified threshold, and/or nonlinearly shrunk towards zero using one of a number of possible frequentist or Bayesian approaches. These result in estimates of the true wavelet coefficients, which would be the wavelet coefficients for the true function if there was no noise. Finally, these estimates are projected back to the original data domain using the IDWT, yielding a denoised nonparametric estimate of the true function. Because most signals may be represented by a small number of wavelet coefficients, yet white noise is distributed equally among all wavelet coefficients, this procedure yields denoised function estimates that tend to retain dominant local features of the function. In this paper, we refer to this property as *adaptive regularization*, since the function is regularized (i.e., denoised or smoothed) in a way that adapts to the characteristics of the function. This property makes the procedure useful for modeling functions with many local features like peaks. Chapters 6 and 8 of Vidakovic (1999) review several different frequentist and Bayesian approaches to wavelet regression.

Most work in wavelet regression to date has been limited to the single-function case, with a few exceptions. Morris, et al. (2003) developed a wavelet-based method for analyzing hierarchical functional data, in which the functions are sampled from a nested hierarchical design. This method produces adaptively regularized estimates and inference for the overall mean function and individual profiles. Morris and Carroll (2004) generalized this work to the functional mixed models setting.

### 3.2 Functional Mixed Models

Suppose we observe  $n$  functional profiles  $Y_i(t), i = 1, \dots, n$ , all defined on the compact set  $\mathcal{T} \in \mathbb{R}^1$ . A functional mixed model for these profiles is given by

$$Y_i(t) = \sum_{j=1}^p X_{ij} B_j(t) + \sum_{k=1}^m Z_{ik} U_k(t) + E_i(t), \quad (2)$$

where  $X_{ij}$  are covariates,  $B_j(t)$  are functional (time-varying) fixed effects,  $Z_{ik}$  are elements of the design matrix for functional random effects  $U_k(t)$ , and  $E_i(t)$  are residual error processes. Here, we assume that  $U_k(t)$  are independent and identically distributed (iid) mean-zero Gaussian processes with covariance surface  $Q(t_1, t_2)$ , and  $E_i(t)$  are iid mean-zero Gaussian processes with covariance surface  $S(t_1, t_2)$ , with  $U_k(t)$  and  $E_i(t)$  being independent. Note that  $Q$  indicates the covariance across the random effect functions  $k = 1, \dots, m$ , and  $S$  indicates the covariance across the residual error processes for the  $n$  curves, after conditioning on the fixed and random effects. Note that the iid assumptions on the individual random effect functions and residual error processes makes Equation (2) a special case of the more general functional mixed model presented in Morris and Carroll (2004). Since the response, fixed effects, random effects, and residual error processes are all functional, heuristically this model can be viewed as fitting separate mixed models at each time point, but with an extra layer added for regularization, i.e. to borrow strength across observations within a function.

Suppose all observed profiles are sampled on the same equally spaced grid  $\mathbf{t}$  of length  $T$ . Let  $Y$  be the  $n \times T$  matrix containing the observed profiles on the grid, with each row containing one observed profile on the grid  $\mathbf{t}$ . A discrete, matrix-based version of this mixed model can be written

$$Y = XB + ZU + E. \quad (3)$$

The matrix  $X$  is an  $n \times p$  design matrix containing (nonfunctional) covariates;  $B$  is a  $p \times T$  matrix whose rows contain the corresponding *fixed effect functions* on the grid  $\mathbf{t}$ .  $B_{ij}$  denotes the effect of the covariate in column  $i$  of  $X$  on the response at time  $t_j$ . The matrix  $U$  is an  $m \times T$  matrix whose rows contain *random effect functions* on the grid  $\mathbf{t}$ , and  $Z$  is the corresponding  $n \times m$  design matrix. Each row of the  $n \times T$  matrix  $E$  contains the residual error process for the corresponding observed profile. We assume that the rows of  $U$  are iid  $\text{MVN}(\mathbf{0}, Q)$  and the rows of  $E$  are iid  $\text{MVN}(\mathbf{0}, S)$ , independent of  $U$ , with  $Q$  and  $S$  being  $T \times T$  covariance matrices that are discrete approximations to the covariances surfaces in (2) on the grid.

This model is very flexible and can be used to represent a wide range of functional data. The

fixed effect functions may be group mean functions, interaction functions, or functional linear effects for continuous covariates, depending on the structure of the design matrix. The random effect functions provide a convenient mechanism for modeling between-function correlation, for example when multiple profiles are obtained from the same individual. The model places no restrictions on the form of the fixed or random effect functions. Since the forms of the covariance matrices  $Q$  and  $S$  are also left unspecified, it is typically not feasible to fit this model without first making further assumptions.

### 3.3 Wavelet-Based Functional Mixed Models (WFMM)

Morris and Carroll (2004) did not fit model (4) directly, but instead projected the observed profiles into the wavelet space, then worked with the wavelet-space version of the model. This allowed the modeling to be done in a more parsimonious and computationally efficient manner, and enabled a convenient mechanism for adaptively regularizing the fixed effect functions.

The projection is accomplished by applying the discrete wavelet transform (DWT) to each row of  $Y$ , yielding a matrix of wavelet coefficients  $D = YW'$ , where  $W'$  is the DWT projection matrix. Row  $i$  of  $D$  contains the wavelet coefficients for profile  $i$ , with the columns corresponding to individual wavelet coefficients and double-indexed by scale  $j$  and location  $k$ . It is easy to show that the wavelet-space version of model (3) is

$$D = XB^* + ZU^* + E^*, \quad (4)$$

where each row of  $B^* = BW'$  contains the wavelet coefficients corresponding to one of the fixed effect functions, each row of  $U^* = UW'$  contains the wavelet coefficients for a random effect function, and  $E^* = EW'$  contains the wavelet-space residuals. The rows of  $U^*$  and  $E^*$  remain independent mean-zero Gaussians, but with covariance matrices  $Q^* = WQW'$  and  $S^* = WSW'$ .

Motivated by the whitening property of the wavelet transform, many wavelet regression methods in the single-function setting assume that the wavelet coefficients for a given function are mutually independent. Morris and Carroll (2004) effectively make this assumption in the wavelet-based functional mixed model by constraining  $Q^*$  and  $S^*$  to be diagonal. Allowing the

variance components to differ across both wavelet scale  $j$  and location  $k$  yields  $Q^* = \text{diag}(q_{jk})$  and  $S^* = \text{diag}(s_{jk})$ . This assumption reduces the dimensionality of  $Q$  and  $S$  from  $T(T+1)/2$  to  $T$ , while still accommodating a reasonably wide range of nonstationary within-profile covariance structures for both the random effects and residual error processes.

Morris and Carroll (2004) used a Markov Chain Monte Carlo scheme to generate posterior samples for quantities of model (4). Vague proper priors were used for the variance components, and independent mixture priors were used for the elements of  $B^*$ . Specifically, the prior for  $B_{ijk}^*$ , the wavelet coefficient at scale  $j$  and location  $k$  for fixed effect function  $i$ , was

$$\begin{aligned} B_{ijk}^* &= \gamma_{ijk} \text{Normal}(0, \tau_{ij}) + (1 - \gamma_{ijk}) \delta_0 \\ \gamma_{ijk} &\sim \text{Bernoulli}(\pi_{ij}), \end{aligned} \tag{5}$$

with  $\delta_0$  being a point mass at zero. Use of this mixture prior causes the posterior mean estimates of the  $B_{ijk}^*$  to be nonlinearly shrunk towards zero, which results in adaptively regularized estimates of the fixed effect functions. The parameters  $\tau_{ij}$  and  $\pi_{ij}$  are *regularization parameters* that determine the relative trade-off of variance and bias in the nonparametric estimation. They may either be prespecified or estimated from the data using an empirical Bayes method; see Morris and Carroll (2004) for details.

Posterior samples for each fixed effect function,  $\{\mathbf{B}_i^{(g)}, g = 1, \dots, G\}$ , on the grid  $\mathbf{t}$  are obtained by applying the IDWT to the posterior samples of the corresponding complete set of wavelet coefficients  $\mathbf{B}_i^{*(g)} = [B_{i11}^{*(g)}, \dots, B_{iJK_J}^{*(g)}]$ , and similarly for the random effect functions  $\mathbf{U}_i$ . If desired, posterior samples for the covariance matrices  $Q$  and  $S$  may also be computed using matrix multiplication  $Q^{(g)} = WQ^{*(g)}W'$  and  $S^{(g)} = WS^{*(g)}W'$ , respectively. Since  $Q^{*(g)}$  and  $S^{*(g)}$  are diagonal, this may be accomplished in an equivalent but more efficient manner by applying the 2-dimensional version of the IDWT (2d-IDWT) to  $Q^{*(g)}$  and  $S^{*(g)}$  (Vannucci and Corradi, 1999). These posterior samples of the quantities in model (3) may subsequently be used to perform any desired Bayesian inference.

## 4 Handling Incomplete Profiles in WFMM

The method described above cannot be used to analyze data for which some the profiles are incomplete, i.e., not fully observed on the grid  $\mathbf{t}$ , because the first step of the method, the DWT, cannot be applied to incomplete profiles. Under these circumstances, one alternative is to simply perform a "complete case" analysis, using only complete profiles, but this is inefficient since it ignores information contained in the incomplete profiles. This problem is especially severe when a high proportion of observed profiles are incomplete, which is true for the TriTrac accelerometer data from the Planet Health study.

In this section, we introduce two missing data approaches that can be used to incorporate information from the incomplete profiles in the wavelet-based functional mixed model when there are at least some complete profiles available. Both methods involve imputation of "missing wavelet coefficients" from predictive distributions at each iteration of the MCMC. Missing wavelet coefficients are wavelet coefficients for an individual profile, for which the support of the corresponding basis function intersect missing regions of the profile. In the first method, the imputation distributions are defined based on the posterior means of model parameters obtained from an MCMC applied to the complete case data, while in the second, posterior predictive means and variances are used. These approaches are appropriate to use when the data is missing completely at random (MCAR, Little and Rubin, 2002), meaning that the missingness is not related to the observed nor unobserved responses. Craddock, et al. (2004) described a validation study in which they concluded that the missingness in the accelerometer data from the Planet Health study was MCAR.

Suppose we have an incomplete profile,  $Y_i(t)$ , that is observed on the set of times  $\mathbf{t}^O$ , but missing on the set of times  $\mathbf{t}^M$ , with  $\mathbf{t}^O \cup \mathbf{t}^M = \mathbf{t}$ , an equally spaced grid on the region  $\mathcal{T}$ . From (3), the model for  $\mathbf{Y}_i$ , a row vector containing the full profile on the grid  $\mathbf{t}$ , is given by

$$\mathbf{Y}_i = X_i B + Z_i U + \mathbf{E}_i, \quad (6)$$

where  $X_i$  is  $1 \times p$ ,  $B$  is  $p \times T$ ,  $Z_i$  is  $1 \times m$ ,  $U$  is  $m \times T$ , and  $\mathbf{E}_i$  is  $1 \times T$ . The rows of  $U$

are independently distributed as  $\text{Normal}\{0, Q\}$ , and  $\mathbf{E}_i \sim \text{Normal}\{0, S\}$ . Let  $\Omega$  be the vector containing the covariance parameters determining the matrices  $Q$  and  $S$ . The joint distribution of the profile on the grid, conditional on the fixed effects, covariance parameters, and random effects, is  $\{\mathbf{Y}_i | B, \Omega, U\} \sim \text{Normal}(\boldsymbol{\mu}_i, \Sigma_i)$ , with

$$\boldsymbol{\mu}_i = X_i B + Z_i U \quad (7)$$

$$\Sigma_i = S. \quad (8)$$

Partition  $\mathbf{Y}_i = (\mathbf{Y}_i^O \mathbf{Y}_i^M)$ , with  $\mathbf{Y}_i^O = \{Y_i(t) : t \in \mathbf{t}^O\}$  and  $\mathbf{Y}_i^M = \{Y_i(t) : t \in \mathbf{t}^M\}$  being vectors of length  $T_i^O$  and  $T_i^M$  containing the observed and missing regions of the profile, respectively. Similarly partition  $\boldsymbol{\mu}_i = (\boldsymbol{\mu}_i^O \boldsymbol{\mu}_i^M)$  and  $\Sigma_i = \begin{bmatrix} \Sigma_i^{O,O} & \Sigma_i^{O,M} \\ \Sigma_i^{M,O} & \Sigma_i^{M,M} \end{bmatrix}$ . By standard conditional normal calculations, we find that

$$\{\mathbf{Y}_i^M | \mathbf{Y}_i^O, B, \Omega, U\} \sim \text{Normal}(\boldsymbol{\mu}_i^{M|O}, \Sigma_i^{M|O}), \quad (9)$$

with  $\boldsymbol{\mu}_i^{M|O} = \boldsymbol{\mu}_i^M + \Sigma_i^{M,O}(\Sigma_i^{O,O})^{-1}(\mathbf{Y}_i^O - \boldsymbol{\mu}_i^O)$  and  $\Sigma_i^{M|O} = \Sigma_i^{M,M} - \Sigma_i^{M,O}(\Sigma_i^{O,O})^{-1}\Sigma_i^{O,M}$ . We refer to this conditional distribution as the *imputation distribution*. This distribution represents a linear regression of the missing data on the observed parts of the profile.

In the Bayesian paradigm, a natural way to deal with the missing data  $\mathbf{Y}_i^M$  is to treat it as an unknown parameter vector to be updated at each iteration of the MCMC from its complete conditional distribution, which is the imputation distribution (9). While conceptually straightforward, this approach is computationally infeasible here. It requires numerous applications of the DWT and IDWT and extra matrix inversions and multiplications at each iteration of the MCMC, since the missingness is in the data space and the MCMC is applied to the wavelet space version of the model.

A less computationally intensive alternative is to first perform a "complete case analysis" to obtain posterior samples of the model parameters, then use these to characterize the imputation distribution (9). This distribution may then be projected into the wavelet space to yield a distribution from which random draws of the "missing wavelet coefficients" can be taken at each

iteration of the MCMC. This approach does not require any DWTs, IDWTs, or extra matrix inversions or multiplications to be done inside the MCMC.

Following are the specific steps necessary to implement this approach, using the posterior mean estimates from the complete case run to characterize the mean and variance in (9).

1. Fit the wavelet-based functional mixed model to the set of complete profiles  $Y^C$ . Compute  $\hat{B}$ ,  $\hat{U}$ , and  $\hat{S}$ , the posterior mean estimates of the fixed effect functions, random effect functions, and residual covariance matrix using the procedure described in Section 3.3.
2. For each incomplete profile  $Y_i(t)$ ,
  - (a) Compute  $\hat{\boldsymbol{\mu}}_i^{M|O}$  and  $\hat{\Sigma}_i^{M|O}$  in (9), using the posterior mean estimates of the model quantities in place of  $\boldsymbol{\mu}_i$  and  $\Sigma_i$ .
  - (b) Form the mean imputed profile  $M_i(t)$  on the grid  $\mathbf{t}$ ,  $\mathbf{M}_i$ , by setting  $M_i(t) = Y_i(t)$  for  $t \in \mathbf{t}^O$  and  $M_i(t) = \hat{\boldsymbol{\mu}}_i^{M|O}$  for  $t \in \mathbf{t}^M$ .
  - (c) Form the covariance matrix for the imputed profile  $V_i(t_1, t_2)$  on  $\mathbf{t} \times \mathbf{t}$ , by setting  $V_i(t_1, t_2) = \hat{\Sigma}_i^{M|O}(t_1, t_2)$  if  $t_1, t_2 \in \mathbf{t}^M$  and  $V_i(t_1, t_2) = 0$  if  $t_1 \in \mathbf{t}^O$  or  $t_2 \in \mathbf{t}^O$ .
  - (d) Apply the DWT to the mean imputed profile, yielding the corresponding vector of wavelet coefficients,  $\mathbf{M}_i^* = \mathbf{M}_i W'$ , double-indexed by wavelet scale  $j$  and location  $k$ .
  - (e) Apply the 2-d DWT to the covariance matrix for the imputed profile to compute the corresponding covariance matrix of the imputed wavelet coefficients,  $V_i^* = W V_i W'$ . Because of our independence assumption between the wavelet coefficients within a given function, we restrict attention to the diagonal elements of this matrix,  $\mathbf{v}_i^* = \text{diag}(V_i^*)$ . Each element of the vector  $\mathbf{v}_i^*$ ,  $v_{ijk}^*$ , contains the imputation variance for a single wavelet coefficient, double-indexed by scale  $j$  and location  $k$ .
3. Fit the wavelet-based functional mixed model to the full data set, including the complete and incomplete profiles. At each iteration of the MCMC, add a step whereby for each incomplete profile indexed by  $i$ , we draw each wavelet coefficient  $d_{ijk}$  ( $j = 1, \dots, J$ ,  $k =$

$1, \dots, K_j$ ) from its wavelet-space imputation distribution, which is  $\text{Normal}(M_{ijk}^*, v_{ijk}^*)$ . For any "observed" wavelet coefficients for which the corresponding wavelet basis function,  $\psi_{jk}(t)$ , is completely contained within  $\mathbf{t}^O$ , the imputation variance  $v_{ijk}^*$  will be 0 and the imputation mean  $M_{ijk}^*$  will be  $d_{ijk}$ , the wavelet coefficient we would have obtained by applying the DWT to the profile  $\mathbf{Y}_i$  if it were completely observed.

The procedure described above assumes that for each incomplete profile  $\mathbf{Y}_i$ , we have at least one complete profile from that child, since it conditions on estimates of the corresponding child-level random effect function  $U$  from the complete case analysis. When this is not the case, the procedure is easily adapted by substituting  $\boldsymbol{\mu}_i = X_i B$  and  $\Sigma_i = Q + S$  for (7) and (8), respectively. Recall that in our example  $Q$  represents the child-to-child covariance and  $S$  the day-to-day covariance. Inclusion of the child-to-child variability tends to inflate the imputation variances.

This approach has several desirable qualities. It is easy to implement and makes full use of the functional data, borrowing strength both within and between profiles while performing the imputation. The borrowing of strength from within the profile is accomplished through the conditional distribution in (9), and the borrowing of strength between profiles occurs from the use of parameter estimates from the complete case analysis to characterize the distributions in (7) and (8). Because multiple draws are taken from the imputation distribution, the estimated variability of the imputation is propagated throughout any subsequent inference.

However, one weakness of this approach is that by conditioning on the parameter estimates from the complete profile model fit, it fails to propagate the uncertainty of the parameter estimation into the imputation variances. This may be fixed by using posterior predictive distributions instead, which integrate over this uncertainty. That is, replace the conditional mean and covariance in (7) and (8) in the imputation distribution in (9) by the posterior predictive mean and covariance,  $\mu_i^{\text{pred}} = E(\mathbf{Y}_i | Y^C)$  and  $\Sigma_i^{\text{pred}} = \text{var}(\mathbf{Y}_i | Y^C)$ , respectively. Given a set of  $G$  MCMC

samples from the complete profile run, these may be estimated by the following equations:

$$\hat{\mu}_i^{\text{pred}} = G^{-1} \sum_{g=1}^G \mu_i^{(g)} = \hat{\mu}_i \quad (10)$$

$$\hat{\Sigma}_i^{\text{pred}} = \hat{S} + (G - T)^{-1} \sum_{g=1}^G \{\mu_i^{(g)} - \hat{\mu}_i^{\text{pred}}\} \{\mu_i^{(g)} - \hat{\mu}_i^{\text{pred}}\}, \quad (11)$$

with  $\mu_i^{(g)} = X_i B^{(g)} + Z_i U^{(g)}$ , and  $B^{(g)}$  and  $U^{(g)}$  being the posterior samples of  $B$  and  $U$  from iteration  $g$  of the complete case MCMC, and  $\hat{S}$  the posterior mean estimator of the within-function residual covariance matrix  $S$ . Details of the derivations of (10) and (11) are in the appendix.

Note that because of the mixture prior placed on  $B^*$ , the predictive distribution  $f(\mathbf{Y}_i | Y^C)$  is not multivariate normal. Thus, by representing this distribution by its first two moments and using the normal distribution to perform our imputation, we are using an approximation. This keeps the procedure computationally feasible, since sampling from the actual posterior predictive distribution would require multiple DWT and IDWT calculations within the MCMC, as was the case for the complete conditional distribution. Our use of the posterior predictive means and variances improves upon the conditional approach because it propagates the uncertainty due to parameter estimation in the correct manner, as indicated by the second term in (11).

## 5 Analysis of TriTrac Data from Planet Health

### 5.1 Complete Case Analysis

We first modeled the set of complete profiles in order to obtain posterior predictive distributions to characterize the imputation distributions for the missing parts of the incomplete profiles. There were a total of 95 complete daily profiles from 61 children, i.e., had no missing observations between 9am and 8pm. Let  $Y^C$  be the  $95 \times 660$  response matrix, each row of which contained the log accelerometer profile (in log METs) for one day from one child, sampled on the time grid  $\mathbf{t} = \{t_m, m = 1, \dots, 660\}$ , consisting of every minute from 9am to 8pm. We log transformed the data to stabilize the variance and make the data more symmetric to accommodate the Gaussian error assumptions underlying the functional mixed model.

We modeled these data using the functional mixed model (3),  $Y^C = XB + ZU + E$ . The matrix  $X$  was a  $95 \times 13$  design matrix containing child and day-level covariates, and corresponding to the  $13 \times 660$  matrix  $B$ , whose rows were the fixed effect functions on the grid  $\mathbf{t}$ . Entry  $B_{ij}$  described the effect of covariate  $i$  on the activity levels at time  $t_j$ . The matrix  $Z$  was a  $95 \times 61$  design matrix, with corresponding  $61 \times 660$  matrix  $U$ , for which each row contained the random effect function for a single child on the grid  $\mathbf{t}$ . The  $95 \times 660$  matrix  $E$  contained the residual errors on the same grid. We assumed that the rows of  $U$  and  $E$  were mutually independent mean zero Gaussians with  $660 \times 660$  covariance matrices  $Q$  and  $S$ , respectively.

The  $X$  matrix we used included columns corresponding to an overall functional "intercept", a gender effect (=1 if boy, -1 if girl), an effect for higher tricep skinfolds (=1 if  $> 20$ , =-1 if  $\leq 20$ ), a body mass index (BMI) effect, an effect for the average number of hours per day watching television, day-of-week effects, a seasonal effect (=1 if after the beginning of daylight savings time [DST], =0 if before DST), and school effects. All effects were functional, meaning that they were allowed to vary as a function of time of day. Both the BMI and TV hours covariates were treated as continuous, with the BMI covariate mean-centered and the TV hours covariate standardized. School effects were only included for schools B, D, and E, since there were only 1 and 4 complete profiles from schools A and C, respectively, which we determined were not enough to estimate their corresponding school fixed effects.

Written out in scalar form, the model for profile  $i$  at time  $t_j$ ,  $Y_i^C(t_j)$ , was

$$Y_i^C(t_j) = B_0(t_j) + \sum_{k=1}^{12} X_{ik} B_k(t_j) + \sum_{k=1}^{61} Z_{ik} U_k(t_j) + E_i(t_j), \quad (12)$$

where  $U_k(t_j)$  were mean-zero Gaussians with  $\text{cov}\{U_k(t_j), U_{k'}(t_{j'})\} = Q_{jj'}$  if  $k = k'$ , 0 otherwise;  $E_i(t_j)$  were mean-zero Gaussians with  $\text{cov}\{E_i(t_j), E_{i'}(t_{j'})\} = S_{jj'}$  if  $i = i'$ , 0 otherwise; and  $\text{cov}\{U_k(t_j), E_i(t_{j'})\} = 0$  for all  $i, j, j', k$ .

We obtained posterior samples for all parameters in this model using the wavelet-based functional mixed model approach described in Section 3.3. We chose a Daubechies wavelet with 4 vanishing moments (Daubechies 1992), and performed the wavelet decomposition to  $J = 8$  levels. Maximum likelihood estimates were used as starting values for the MCMC for

all model parameters. The regularization parameters were estimated using the empirical Bayes approach described in Morris and Carroll (2004), and vague proper priors were used for the variance components. After a burn-in of 1000, we obtained 20,000 MCMC samples of the model parameters, keeping every  $10^{th}$ . This took roughly 7 hours to run on our Xeon 3.2 GHz Windows 2000 machine with 2GB RAM, and the posterior samples occupied roughly 300MB. Trace plots and Metropolis-Hastings acceptance probabilities, available from the first author, indicated that the MCMC had good convergence properties.

## 5.2 Imputation Distributions for Incomplete Profiles

We used these posterior samples to estimate the posterior predictive means and variances for each incomplete profile,  $\hat{\mu}_i^{pred}$  and  $\hat{\Sigma}_i^{pred}$  in (10) and (11). As described in Section 4, we used these estimates as the basis for regressing the missing data on the observed parts of the profile to obtain imputation distributions for the missing data, which had mean  $\hat{\mu}_i^{M|O}$  and covariance matrix  $\hat{\Sigma}_i^{M|O}$ .

Figure 4 contains six incomplete profiles, with their missing regions replaced by the mean and 95% pointwise bounds of their imputation distributions. Note how the imputation distributions borrow strength from nearby observations and tend to "connect" the imputed data with nearby observed data. They also allow the magnitude of the nearby observed data to play a role in the imputation. Also note that the imputation variances tend to be smaller for the values immediately adjacent to observed values, and in regions of the curves with less variability in the population.

Using the DWT, we projected these imputation distributions into the wavelet space. At each iteration of the MCMC applied to the full data set, we took random draws from this distribution to fill in the "missing wavelet coefficients."

## 5.3 Model for Analysis of Full Data Set

We used the same underlying model for the full data analysis as for the complete case analysis, except we removed the functional intercept term and allowed each school to have its own fixed

effect function, since the full data set contained enough profiles to reliably estimate them all.

We obtained posterior samples for all parameters in this model using an MCMC, with the missing wavelet coefficients sampled from their imputation distributions at each iteration, as described in Section 4. As in the complete case analysis, we chose a Daubechies wavelet with 4 vanishing moments, and performed the wavelet decomposition to  $J = 8$  levels. The regularization parameters were estimated using the empirical Bayes approach described in Morris and Carroll (2004), and are available by request from the first author. Vague proper priors were used for the variance components. We ran four parallel chains, each with a burn-in of 1000 and consisting 2500 MCMC samples, keeping every 5. Maximum likelihood estimates were used as starting values for the MCMC for all model parameters in each chain. This took roughly 40 hours to run on our Xeon 3.2 GHz Windows 2000 machine with 2GB RAM, and the posterior samples occupied roughly 300MB. For 87% of the variance components, the Metropolis-Hastings acceptance probabilities were between 0.25 and 0.50. The histogram of Metropolis-Hastings acceptance probabilities and trace plots are available as supplementary material from the first author, and indicate that the MCMC had good convergence properties.

## 5.4 Results

### 5.4.1 Analysis of Fixed Effect Functions

To consider the marginal time of the day effect on activity levels, we computed the overall mean curve by equally weighting each of the schools' fixed effects functions and conditioning on the mean values of all other covariates. Figure 5 contains the posterior mean and 90% posterior pointwise credible bounds for the overall mean curve. Throughout the school day, the curve is characterized by numerous spikes that indicate periods of time of coordinated activity, e.g., class switches and lunch periods for the different schools. There is a large spike between 2:15pm and 3:00pm corresponding to the end of the school day. The mean activity profiles are less spiky after school, indicating less coordinated activity across days and children. The mean activity levels remained relatively constant from 3:00pm to 6:30pm, then decreased later in the evening.

For each fixed effect function, we plotted the posterior mean curve and computed pointwise

90% posterior bounds. Figure 6 contains these curves for four fixed effect functions of interest; other curves are available by request from the first author. Recall that in our model, the effects are additive on the log scale, so they are multiplicative on the MET scale. One may obtain the multiplicative effects by exponentiating the values in these plots. These multiplicative effects may then be converted into percent increases or decreases in the MET scale.

To further summarize the results, we computed the average percent increases/decreases corresponding to each fixed effect function, aggregating within the following time intervals, chosen based on the overall mean curve: (1) all day, 9am-8pm; (2) morning, 9am-11:30am; (3) lunch, 11:30am-12:30pm; (4) afternoon, 12:30pm-2:15pm; (5) going home, 2:15pm-3:00pm; (6) after school, 3:00pm-5:30pm; (7) early evening, 5:30pm-7:00pm; and (8) late evening, 7:00pm-8:00pm. We also computed the 90% credible intervals for these quantities, reported in square brackets. We report some of these results here; the full set of results is available by request from the first author.

The fixed effect curves for the different schools were characterized by numerous peaks present throughout the school day. These were most evident for school E; see Figure 6(a). This school provided the most daily profiles in this data set (146 out of 292), and it appeared to have the most regular schedule of the schools in the study; see Figure 2. The regular pattern of peaks reveals the school’s class schedule. The large peaks in the morning and afternoon are exactly 48 minutes apart, and indicate class switches. The three peaks around noon are 24 minutes apart, and likely indicate different lunch periods. From the large extended spike in the afternoon, we surmise that school let out around 2:15pm. Although regular peaks were evident in the school’s main effect curve, they were not obvious in any individual curve because of the high levels of day-to-day and child-to-child variability. This can be seen in the bottom two panels of Figure 1, which contain profiles from a child at this school.

Investigating the day-of-week effects, we found that children tended to be less active on Tuesdays (3.3% decrease [-6.2%, -0.2%]), Thursdays (2.9% decrease [-5.5%, -0.2%]), and Fridays (3.6% decrease [-6.8%, -0.4%]), compared to Mondays, aggregating over the entire day. These effects

were especially strong during the after-school period (3:00-5:30, Tuesday -7.7% [-12.6%, -2.2%], Thursday -7.8% [-12.5%, -3.1%], Friday -5.8% [-11.4%, -0.1%]) A similar but less pronounced trend was present on Wednesdays (overall 1.9% decrease [-5.0%, 1.4%], after school 5.1% decrease [-10.5%, 0.9%]).

In 1997, daylight savings time (DST) in Boston started on April 6th. In our analysis, we found that the activity levels were generally higher in profiles obtained after DST than before DST (overall 8.2% increase [-0.5%, 18.1%]). See Figure 6(c). This effect was especially strong as school was letting out (2:15-3:00, 25% increase [4.2%, 53.4%]) and in the early evening (5:30-7:00, 29.5% increase, [5.6%, 59.2%] ), a time period during which the sun was still out after DST, but had already set before DST.

We considered the effects of various child-level covariates. There was strong evidence of a significant body mass index (BMI) effect throughout the day (4.3% increase in activity levels for every unit of BMI above the average [2.8%, 5.8%]). See Figure 6(b). There was no evidence of any difference in activity levels between children with tricep skinfold caliper values above or below 20. Boys tended to be slightly more active than girls, on average, most notably over lunch (4.8% increase [0.5%, 9.1%]).

Figure 6(d) contains the posterior mean curve corresponding to the covariate mean number of hours per day watching TV. Since we modeled the standardized version of this covariate, this curve represents the amount added to (or subtracted from) the mean log activity curve for each standard deviation unit above (or below) the mean. Overall, children who tended to watch more TV tended to also be less active (1.3% decrease per standard deviation unit [-2.4%, -0.1%]). This effect was especially strong just after school (3:00-5:30, 2.6% decrease [-4.6%, -0.5%]) and in the late evening (7:00-8:00, 3.6% decrease [-6.1%, -1.1%]). For example, a child whose average TV watching was 2 standard deviations above the mean ( $\approx 8$  hours/day) was on average 11% less active from 7-8pm on a weekday evening than a child whose average TV watching was 1 standard deviation below the mean ( $\approx 1$  hour/day). Interestingly, children watching more TV tended to be more active at lunch (2.7% increase per standard deviation unit [0.4%, 5.2%]).

### 5.4.2 Variance Component Analysis

We summarized the relative variability from day to day by  $\rho = \text{Tr}(S) / \{\text{Tr}(Q) + \text{Tr}(S)\}$ , where  $\text{Tr}(Q)$  and  $\text{Tr}(S)$  were the traces of the child-to-child covariance matrix  $Q$  and day-to-day covariance matrix  $S$ . The posterior mean estimate of  $\rho$  was 90.9%, indicating that 90.9% of the variability in the log accelerometer profiles was day to day, while the remaining 9.1% was from child to child. The 90% posterior credible interval for  $\rho$  was [88.8%, 92.8%].

To evaluate how these sources of variability varied over  $t$ , we considered the child-to-child and day-to-day variances as a function of  $t$ ,  $V_q(t) = Q(t, t)$  and  $V_s(t) = S(t, t)$ , respectively (plots not shown). We found that the child-to-child variability was greater during the school day than after school, while the day-to-day variability was greater after school than during the school day. Computing the relative variability from day to day as a function of time of the day,  $\rho(t) = V_s(t) / \{V_q(t) + V_s(t)\}$ , we found that the percent of variability from day to day increased from 85-90% during the school day up to 95-99% after 3pm.

### 5.4.3 Assessing Bouts

In the literature on accelerometer data, there has been a great deal of interest in studying "bouts," or short bursts of intense activity. Here, we considered bouts to be periods of time during which the child was engaging in moderate or vigorous activity, which corresponded to activity levels of greater than 3.0 MET (Rowlands et al. 2004). In the existing literature, the data analysis performed frequently includes estimating the probabilities of bouts for different groups of individuals. In our wavelet-based functional mixed model approach, we did not directly model these probabilities, but the unified Bayesian framework underlying the method made it easy to compute these probabilities as a function of the time of day for any group of individuals using the posterior samples output from the MCMC.

Given a child with covariate levels  $\mathbf{X}^*$ , the posterior predictive probability that they experience a bout at time  $t$  in a hypothetical future daily activity profile  $\mathbf{Y}^*(t)$  is given by

$$\phi_{\text{WFMM}}(t) = \text{Pr}\{\mathbf{Y}^*(t) > 3.0 | \mathbf{Y}, \mathbf{X}^*\}$$

$$= \int I\{\mathbf{Y}^*(t) > 3.0\} f\{\mathbf{Y}^*(t)|\theta, \mathbf{X}^*\} f(\theta|Y) d\theta, \quad (13)$$

where  $\theta = \{B, Q, S\}$  are the fixed effect and covariance parameters in the model, and  $Y$  are the profiles we used to fit the model. Expression (13) can be estimated from the  $G$  posterior samples  $\theta^{(g)} = \{B^{(g)}, Q^{(g)}, S^{(g)}\}, g = 1, \dots, G$ , obtained from the MCMC, by  $\hat{\phi}_{\text{WFMM}}(t) = G^{-1} \sum_{g=1}^G \Phi[\{3.0 - \mu^{(g)}(t)\}/\sigma^{(g)}(t)]$ , where  $\mu^{(g)}(t) = \mathbf{X}^* B^{(g)}(t)$ ,  $\sigma^{(g)}(t) = \sqrt{Q^{(g)}(t, t) + S^{(g)}(t, t)}$ , and  $\Phi(x)$  is the standard normal cdf evaluated at  $x$ .

We computed the probability of bouts as a function of the time of the day for Thursdays before DST for children from school E. This curve is given by the dotted-dashed line in Figure 7. To check how well our model captured these bouts, we also computed an empirical estimate of the probability of bouts for each time point averaging over the  $n = 42$  accelerometer profiles obtained on Thursdays before DST from children enrolled at school E. The raw empirical estimator was  $\hat{\phi}_{\text{EMP}}(t) = n^{-1} \sum_{i=1}^n I(Y_i(t) > 3.0)$ . The solid line in Figure 7 is a wavelet-denoised version of this curve, denoised using *Sureshrink* (Donoho and Johnstone, 1995). Although we did not directly model the probability of bouts, our wavelet-based functional mixed model appeared to do a reasonable job of capturing these features of the data.

## 6 Discussion

We first discuss the specific results of our analysis, and then assess the fitness of the wavelet-based functional mixed model for analyzing accelerometer data.

The positive body mass index (BMI) effect that we observed was initially surprising to us. We had expected that children with higher BMI would be less, not more active. However, results linking obesity and activity levels in existing literature are ambivalent, with different studies reporting positive, negative, or no relationship (Rowlands et al. 2000). Also, note that our analysis was done on the MET scale, which involved converting the TriTrac's raw acceleration counts to the energy scale then adjusting for the child's basal metabolic rate using formulas based on the child's gender and weight (see Section 2). Since these formulas are only approximations, it is possible that this effect is at least partly due to imprecision in converting

from the acceleration to MET scales. This should be further explored, and considered in future studies when deciding whether the raw acceleration or MET scales should be used in studying children’s activity levels.

We were not surprised by the large daylight savings time (DST) effect we observed in the data. Considering the weather in Boston, naturally children tended to be more active after April 6th than before April 6th. In 1997, the sun set in Boston at times ranging from 5:10pm to 6:15pm from February 10th through April 5th, then from 7:16pm through 8:11pm from April 6th through May 28th. This may explain the very large spike in the DST effect between 5pm and 7pm. Also matching our intuition was the result that children who tended to watch more television also tended to be less active, and naturally the effect was especially strong just after school (from 3:00-5:30) and in the late evening (after 7:00), typical times for television watching. We found it interesting that an effect in the opposite direction was observed during the lunch period. Perhaps the children who watched more TV at home in the evenings had energy that needed to be released at some time during the day, and lunch was their best opportunity to do it.

In our relative variability analysis, we found that after adjusting for the covariates, including school, the day-to-day variability dominated the child-to-child variability, especially during the after-school hours. In other words, the difference between the average log profiles of a very active and very inactive child with the same covariate levels is small compared to the variability in activity for a given child from day to day, especially after school. This suggests that it is important to get many days per child in order to accurately quantify each child’s typical level of activity. While it is already typical in these studies to monitor each child for 4 to 8 days, it may be a better design to obtain even more days per child, especially if this does not result in much increase in cost for the study.

While not directly modeling the bouts, the wavelet-based functional mixed model can be used to obtain estimates of the probability of bouts at different times of the day for children with different levels of the covariates. It appears that this model does a reasonable job of

capturing these bouts, indicating that it is at least somewhat effective in modeling some of the tail behavior in the distributions. However, there is some evidence of attenuation in our model-based estimates of these probabilities, especially during the after-school period in which there is less coordinated activity and more day-to-day variability. These may be related to our underlying assumptions of normality and equal covariances across different groups of children. It is possible in our framework to allow different covariance parameters across different groups of children, and to relax the normality assumptions using scale mixtures of normals (see Andrews and Mallows, 1974). These adaptations would accommodate heavier tails, which may do an even better job of capturing these bouts.

The wavelet-based functional mixed model is a powerful tool for analyzing accelerometer data. It allows one to consider the joint functional effects of multiple covariates, and has the ability to model correlations between profiles obtained from the same individual using random effect functions. The functions are allowed to be of arbitrary form, and the within-function covariances are allowed to be nonstationary. The fixed effect functions are adaptively regularized using the principles of wavelet shrinkage. Less adaptive methods using kernels or splines would result in more attenuation of dominant local features in the fixed effects curves, possibly resulting in reduced power for inference.

It is also possible to introduce other random effect functions to account for covariance due to other clustering factors, such as school or neighborhood. In this analysis, we chose to model the schools using fixed effects because there were so few of them, but given more schools, we could use random effects. It would be a good idea to use more schools in these studies, since the school-to-school variability appears to be large, and it would be interesting and important to study a wider range of schools with different socioeconomic makeups.

Our model is linear in that we assume the effects are linear in the covariates. It would be interesting to consider generalizing or testing this assumption. However, this framework is still very flexible since the linear coefficients are allowed to be time-varying, and their functional form over time is left arbitrary. A much less flexible model, for example, would be to allow the overall

mean function to be arbitrary, but to force the fixed effects to be constant over time. It would be interesting to develop formal testing procedures for testing whether it is necessary to allow the coefficient to be time-varying for a given covariate; this is a topic for future investigation.

Also, we note that this model is very flexible in its representation of the covariances of the profiles from day to day,  $S$ , and the covariances of the random effect profiles from child to child,  $Q$ . Our assumption of independence in the wavelet space reduces the dimensionality of these covariances from  $T(T+1)/2$  to  $T$ , yet accommodates a reasonably wide range of nonstationary covariance structures. Different variance components are estimated for each wavelet coefficient, which allows the day-to-day and child-to-child variability to differ across both scale and location. This accommodates various types of nonstationarity, allowing the day-to-day and child-to-child variances across profiles to vary over time, and also allowing the level of smoothness in the random effect functions and residual error processes to vary over time.

The missing data methods introduced in this paper allow the wavelet-based functional mixed model to be applied to data with incomplete profiles, which are commonly encountered in accelerometer data. In our case study, these methods allowed us to increase the number of profiles in the analysis by a factor of three. The resulting gain in precision is evident if one compares the posterior bounds from the full data and complete case analyses (not shown).

The wavelet-based functional mixed model method possesses some weaknesses and limitations. It is based on linear models, and so assumes additive errors (in our case study, additive on the log scale). Other types of variability may not be adequately picked up by these models. The normality assumption is somewhat restrictive, although as previously mentioned this could be relaxed using scale mixtures. As is true with nonfunctional mixed models, some models can be unstable to fit, especially when there is near-collinearity in the design matrices, or small effective sample sizes for some of the variance components. These problems are exacerbated in the functional context, since we are effectively fitting  $T$  simultaneous scalar mixed models. Also, it would be useful to have a global functional test for more formally assessing the significance of the fixed effect functions; this is an area we will investigate in the near future. The method

is computationally and memory intensive; the analyses performed for this paper took a total of about 50 computer hours. However, this is not unreasonable considering the time it takes to collect the data. The method is also highly parallelizable, so it could be done in much less time whenever parallel computing resources are available.

While computationally intensive, the method is straightforward to implement. The minimal information one must specify to use our scripts are the  $Y$ ,  $X$ , and  $Z$  matrices, the wavelet basis, the number of levels of decomposition, the number of MCMC samples, and the burn-in. By default, maximum likelihood starting values, empirical Bayes regularization parameters, Fisher’s information-based proposal variances for the Metropolis-Hastings, and vague priors on the variance components are automatically computed.

Although straightforward to implement, this method is considerably complex, combining wavelets with mixed models and wrapping it all up inside a Markov Chain Monte Carlo. This begs the question of what all this complexity buys, of what this method can do that simpler approaches cannot. This functional data modeling approach can be used to perform the same types of standard analyses found in the existing literature, including analyses of average daily activity levels, 30-minute averages, and probabilities of bouts for different groups of individuals, but these can be done more efficiently because we can effectively incorporate incomplete profiles into the analysis. More importantly, the functional approach opens a whole new level of possibilities in terms of analyses that can be done and types of information that can be extracted from these rich data, for example, allowing us to perform inference on time-varying effects. Given the posterior samples from our model fit, we can perform nearly any type of inference we desire, functional or pointwise, on fixed effect functions, random effect functions, or covariance functions. The Bayesian approach propagates the uncertainty from the different sources of variability in the model and the different parameters estimated throughout any subsequent inference.

The wavelet-based functional mixed model, supplemented with the missing data methods introduced in this paper, comprises a promising tool for extracting information from accelerometer

data in activity level studies.

## Acknowledgements

Jeffrey Morris was supported by the National Cancer Institute(CA-107304), Louise Ryan was supported by CA-48061, and Brent Coull was supported by ES012044. Steven Gortmaker was supported by: National Institutes of Child Health and Human Development (HD-30780), and the Centers for Disease Control and Prevention (Prevention Research Centers Grants U48/CCU115807 and U48/DP00064-00S1).

## References

- Abbott, A. P. and Davies, P. S. (2004), "Habitual Physical Activity and Physical Activity Intensity: Their Relation to Body Composition in 5.0-10.5-y-old Children," *European Journal of Clinical Nutrition*, 58(2), 285-291.
- Algase, D. L., Beattie, E., Leitsch, S. A., and Beel-Bates, C. A. (2003), "Biomechanical Activity Devices to Index Wandering Behavior in Dementia," *American Journal of Alzheimer's Disease and other Dementias*, 18(2), 85-92.
- Andrews, D. F. and Mallows, C. L. (1974), "Scale Mixtures of Normal Distributions," *Journal of the Royal Statistical Society, Series B*, 36: 99-102.
- Burrus, C. S., Gopinath, R. A., and Guo, H. (1998), *Introduction to Wavelets and Wavelet Transforms: A Primer*. Upper Saddle River, NJ: Prentice Hall.
- CDC (2000), "Promoting Better Health for Young People Through Physical Activity and Sports: A Report to the President from the Secretary of Health and Human Services and the Secretary of Education, Technical Report, Centers for Disease Control and Prevention.
- CDC NCCDPHP (2001), "Physical Activity and Good Nutrition, Essential Elements to Prevent Chronic Disease and Obesity, at a Glance 2001," Technical Report, Centers for Disease Control and Prevention.
- Coleman, K. J., Saelens, B. E., Wiedrich-Smith, M. D., Finn, J. D., and Epstein, L. H. (1997), "Relationships Between TriTrac-R3D Vectors, Heart Rate, and Self-Report in Obese Children," *Medicine and Science in Sports and Exercise*, 29(11), 1535-1542.
- Cradock, A. L., Weicha, J. L., Peterson, K. E., Sobol, A. M., Colditz, G. A., and Gortmaker, S. L. (2004), "Youth Recall and TriTrac Accelerometer Estimates of Physical Activity Levels," *Medicine and Science in Sports and Exercise*, 36(3), 525-532.
- Daubechies, I. (1992), *Ten Lectures on Wavelets*, Philadelphia, PA: Society for Industrial and Applied Mathematics.

- Dietz W. H. (1998), "Health Consequences of Obesity in Youth: Childhood Predictors of Adult Disease," *Pediatrics*, 101, 518-558.
- Donoho, D. L. and Johnstone, I. M. (1995), "Adapting to Unknown Smoothness via Wavelet Shrinkage," *Journal of the American Statistical Association*, 90, 1200-1224.
- Epstein, L. H., Paluch, R. A., Coleman, K. J., Vito, D., and Anderson, K. (1996), "Determinants of Physical Activity in Obese Children Assessed by Accelerometer and Self-Report," *Medicine and Science in Sports and Exercise*, 28(9), 1157-1164.
- Going, S., Thompson, J., Cano, S., Stewart, D., Stone, E., Harnack, L., Hastings, C., Norman, J., and Corbin, C. (2003), "The Effects of the Pathways Obesity Prevention Program on Physical Activity in American Indian Children," *Preventive Medicine*, 37(6), S62-S69.
- Goldfield, G. S., Kalakanis, L. E., Ernst, M. M., and Epstein, L. H. (2000), "Open-loop Feedback to Increase Physical Activity in Obese Children," *International Journal of Obesity and Related Metabolic Disorders*, 24(7), 888-892.
- Gortmaker, S. L. (2002), "The Role of Physical Activity Environment in Obesity Among Children and Adolescents in the Industrialized World," *Obesity in Childhood and Adolescents*, eds. C. Chen and W. H. Dietz, Nestle Nutrition Workshop Series, Pediatric Program, Vol. 49. Nestec Ltd., Philadelphia: Vevey/Lippencott Williams & Wilkins.
- Gortmaker, S. L., Peterson, K., Wiecha, J., Sobol, A., Dixit, S., Fox, M., and Laird, N. (1999), "Reducing Obesity via a School-Based Interdisciplinary Intervention among Youth: Planet Health," *Archives of Pediatric and Adolescent Medicine*, 153, 409-418.
- Goswami, J. C. and Chan, A. K. (1999), *Fundamentals of Wavelets. Theory, Algorithms and Applications*. New York, NY: Wiley.
- Laird, N. and Ware, J. H. (1982), "Random-Effects Models for Longitudinal Data," *Biometrics*, 38, 963-974.
- Little, R. J. A. and Rubin D. B. (2002), *Statistical Analysis with Missing Data*. Hoboken, NJ: Wiley.
- Matthews, C. E. and Freedson, P. S. (1995), "Field Trial of a Three-Dimensional Activity Monitor: Comparison with Self-Report," *Medicine and Science in Sports and Exercise*, 27(7), 1071-1078.
- Morris, J. S. and Carroll, R. J. (2004), "Wavelet-Based Functional Mixed Models," Technical Report, University of Texas MD Anderson Cancer Center Department of Biostatistics and Applied Mathematics, UTMDABTR-006-04.
- Morris, J. S., Vannucci, M., Brown, P. J., and Carroll, R. J. (2003), "Wavelet-Based Non-parametric Modeling of Hierarchical Functions in Colon Carcinogenesis," *Journal of the American Statistical Association*, 98, 573-597.
- Pearce, K. D. (1999), "Race, Ethnicity, and Physical Activity," *Leisure Today JOPERD*, 70(1), 25-28.
- Ramsay, J. O. and Silverman (1997), *Functional Data Analysis*. New York: Springer.
- Recommended Dietary Allowances* (2000), 10th ed. Washington, DC: National Academy Press.

- Rowlands, A. V., Eston, R. G., and Ingledew, D. K. (1999), "Relationship between Activity Levels, Aerobic Fitness, and Body Fat in 8- to 10-yr-old Children," *Journal of Applied Physiology*, 86(4), 1428-1435.
- Rowlands, A. V., Ingledew D. W., and Eston, R. G. (2000), "The Effect of Type of Physical Activity Measure on the Relationship Between Body Fatness and Habitual Physical Activity in Children: A Meta Analysis," *Annals of Human Biology*, 27(5), 479-497.
- Rowlands, A. V., Thomas, P. W., Eston, R. G., and Topping R. (2004), "Validation of the RT3 Triaxial Accelerometer for the Assessment of Physical Activity," *Medicine and Science in Sports and Exercise*, 36(3), 518-524.
- Strauss, R. S., Rodzilshy D., Burack, G., and Colin, M. (2001), "Psychosocial Correlates of Physical Activity in Healthy Children," *Archives of Pediatrics and Adolescent Medicine*, 155(8), 897-902.
- Talbot, L. A., Gaines, J. M., Huynh, T. N., and Metter, E. J. (2003), "A Home-Based Pedometer-Driven Walking Program to Increase Physical Activity in Older Adults with Osteoarthritis of the Knee: A Preliminary Study," *Journal of the American Geriatric Society*, 51(3), 387-392.
- Vannucci, M., and Corradi, F. (1999), "Covariance Structure of Wavelet Coefficients: Theory and Models in a Bayesian Perspective," *Journal of the Royal Statistical Society, Series B*, 61, 971-986.
- Vidakovic, B. (1999), *Statistical Modeling by Wavelets*, New York: Wiley.
- Westerterp, K. R. (1999), "Physical Activity Assessment with Accelerometers," *International Journal of Obesity and Related Metabolic Disorders*, 23 Suppl 3, S45-S49.
- Westerterp, K. R. (2002), "Pattern and Intensity of Physical Activity," *Nature*, 410, 539.

## Appendix A: Derivation of Posterior Predictive Means and Covariances

Suppose  $Y^C$  is an  $N^C \times T$  matrix whose rows contain  $N^C$  complete profiles, observed on an equally spaced grid  $\mathbf{t}$  of length  $T$ . Assume this matrix is modelled using the functional mixed model (3) with parameters  $\Theta = \{B, U, Q, S\}$ . Let  $\mathbf{Y}_i$  be another profile following the same model that is independent of each profile in  $Y^C$  conditional on  $\Theta$ . Here we show that, given a set of  $G$  posterior samples of  $(\Theta|Y^C)$ , we can estimate the posterior predictive mean  $\mu_i^{\text{pred}} = E(\mathbf{Y}_i|Y^C)$  and covariance matrix  $\Sigma_i^{\text{pred}} = \text{VAR}(\mathbf{Y}_i|Y^C)$  by the expressions in (10) and (11), which are

$$\hat{\mu}_i^{\text{pred}} = G^{-1} \sum_{g=1}^G \mu_i^{(g)} = \hat{\mu}_i \quad (\text{A.1})$$

$$\hat{\Sigma}_i^{\text{pred}} = \hat{S} + (G - T)^{-1} \sum_{g=1}^G \{\mu_i^{(g)} - \hat{\mu}_i^{\text{pred}}\}' \{\mu_i^{(g)} - \hat{\mu}_i^{\text{pred}}\}, \quad (\text{A.2})$$

with  $\mu_i^{(g)} = X_i B^{(g)} + Z_i U^{(g)}$ ;  $B^{(g)}$  and  $U^{(g)}$  are posterior samples of  $B$  and  $U$  from iteration  $g$  of the MCMC performed on  $Y^C$ , and  $\hat{S}$  is the posterior mean estimator of the within-function residual covariance matrix  $S$ .

We start by showing (A.1). First, it is easy to show using alternating conditional expectation arguments that if  $X$  and  $Y$  are independent, conditional on  $Z$ , then  $E(X|Y) = E_{Z|Y}\{E(X|Z)\}$ . Since  $\mathbf{Y}_i$  and  $Y^C$  are independent conditional on  $\Theta$ , this means that  $\mu_i^{\text{pred}} = E_{\Theta|Y^C}\{E(\mathbf{Y}_i|\Theta)\} = E_{\Theta|Y^C}\{X_i B + Z_i U\}$ . Estimating this expectation using the MCMC samples of  $\Theta$ , we get  $\hat{\mu}_i^{\text{pred}} = \hat{\mu}_i$ .

To show (A.2), we first note that alternating conditional expectation arguments can be used to show that if  $X$  and  $Y$  are independent, conditional on  $Z$ , then  $\text{var}(X|Y) = E_{Z|Y}\{\text{VAR}(X|Z)\} + \text{var}_{Z|Y}\{E(X|Z)\}$ . This means that we can write

$$\Sigma_i^{\text{pred}} = \text{var}(\mathbf{Y}_i|Y^C) = E_{\Theta|Y^C}\{\text{var}(\mathbf{Y}_i|\Theta)\} + \text{var}_{\Theta|Y^C}\{E(\mathbf{Y}_i|\Theta)\}. \quad (\text{A.3})$$

Consider the first term in (A.3). Since  $\text{var}(\mathbf{Y}_i|\Theta) = S$ , this term can be estimated by  $\hat{S}$ , the posterior mean estimator of  $S$  computed from the MCMC samples. This gives the first term in (A.2).

Now consider the second term in (A.3). We can write

$$\begin{aligned} \text{var}_{\Theta|Y^C}\{E(\mathbf{Y}_i|\Theta)\} &= E_{\Theta|Y^C}[E(\mathbf{Y}_i|\Theta) - E_{\Theta|Y^C}\{E(\mathbf{Y}_i|\Theta)\}]'[E(\mathbf{Y}_i|\Theta) - E_{\Theta|Y^C}\{E(\mathbf{Y}_i|\Theta)\}] \\ &= E_{\Theta|Y^C}[\{X_i B + Z_i U\} - \mu_i^{\text{pred}}]'[\{X_i B + Z_i U\} - \mu_i^{\text{pred}}], \end{aligned}$$

This expression can be estimated using the MCMC samples by  $(G - T)^{-1} \sum_{g=1}^G \{\mu_i^{(g)} - \hat{\mu}_i^{\text{pred}}\}' \{\mu_i^{(g)} - \hat{\mu}_i^{\text{pred}}\}$ , which is the second part of (A.2).

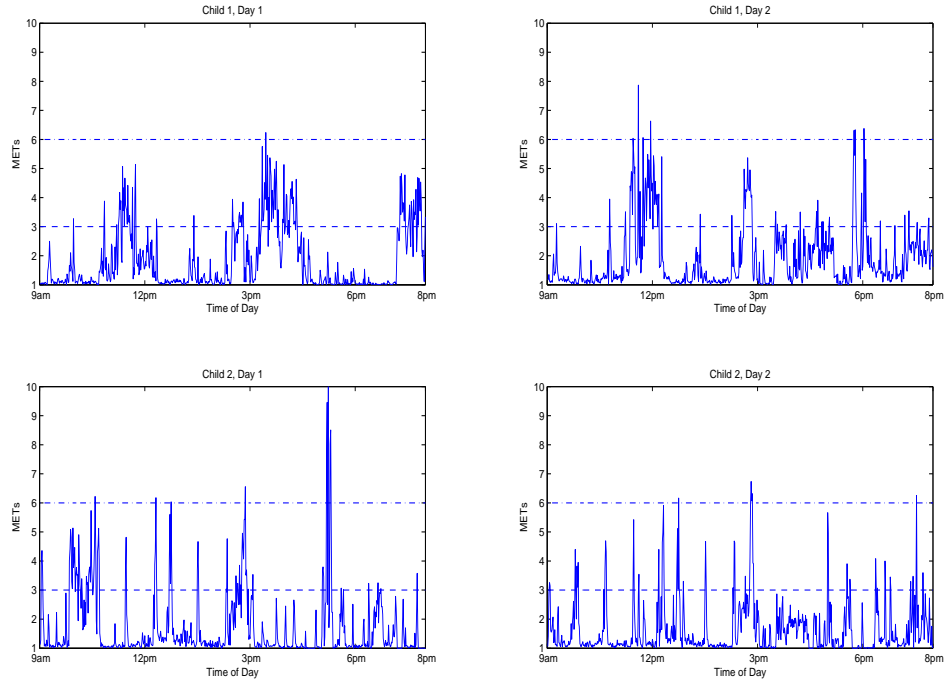


Figure 1: Sample profiles from 2 days for 2 different children, from 9am to 8pm. Activity levels above 6 MET are considered vigorous, while activity levels between 3 and 6 MET are moderate.

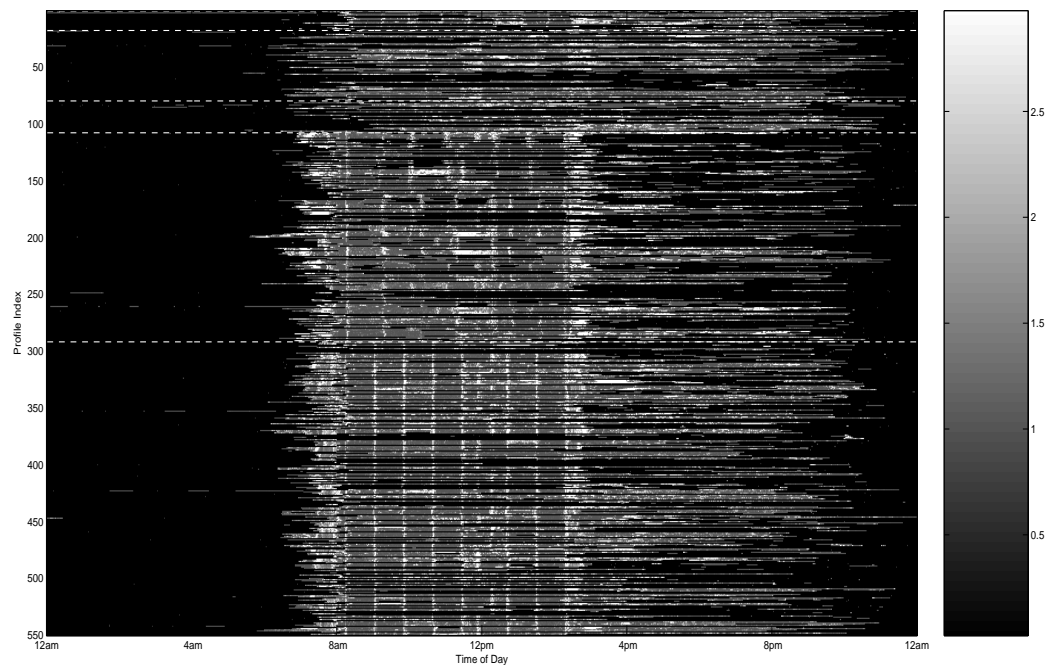


Figure 2: Heat map of all weekday accelerometer profiles. The rows are the daily profiles, ordered by school and child within school. The columns are the minutes of the day, from 12:01am through 12:00 midnight. The minimum activity level registered on the accelerometer is 1 MET. The black regions of the plot indicate regions of the profiles where the activity level is missing. The white regions indicate bouts, or regions where the activity profile is  $> 3.0$  MET. The dotted white lines mark the divisions between profiles from different schools.

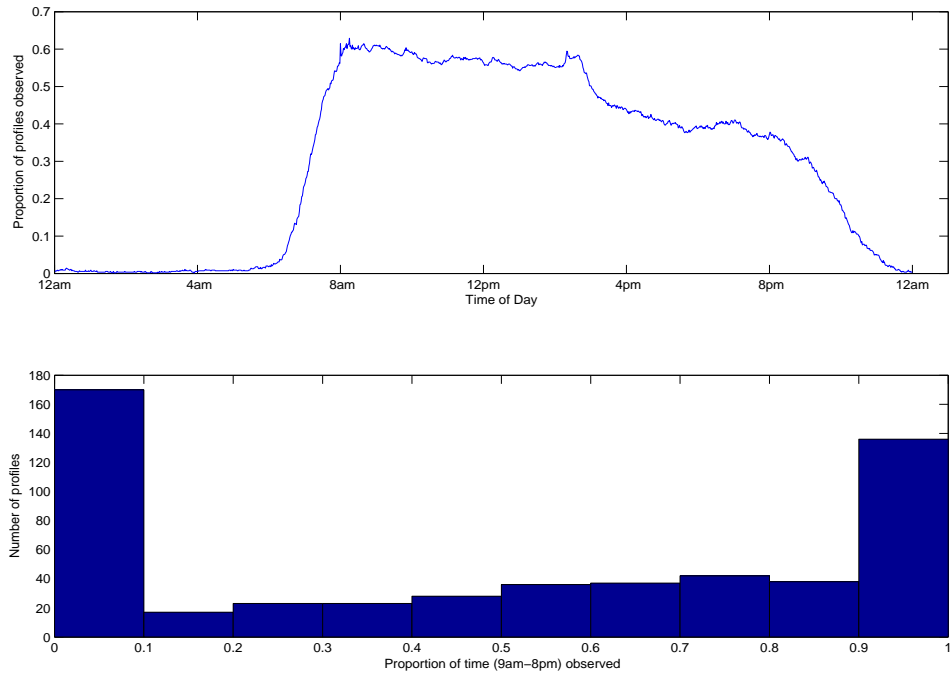


Figure 3: Summary of missingness in the data. The top curve summarizes the proportion of daily profiles observed (i.e., nonmissing) as a function of the time of day. The bottom is a histogram summarizing the proportion of time between 9am and 8pm that is observed for each profile.

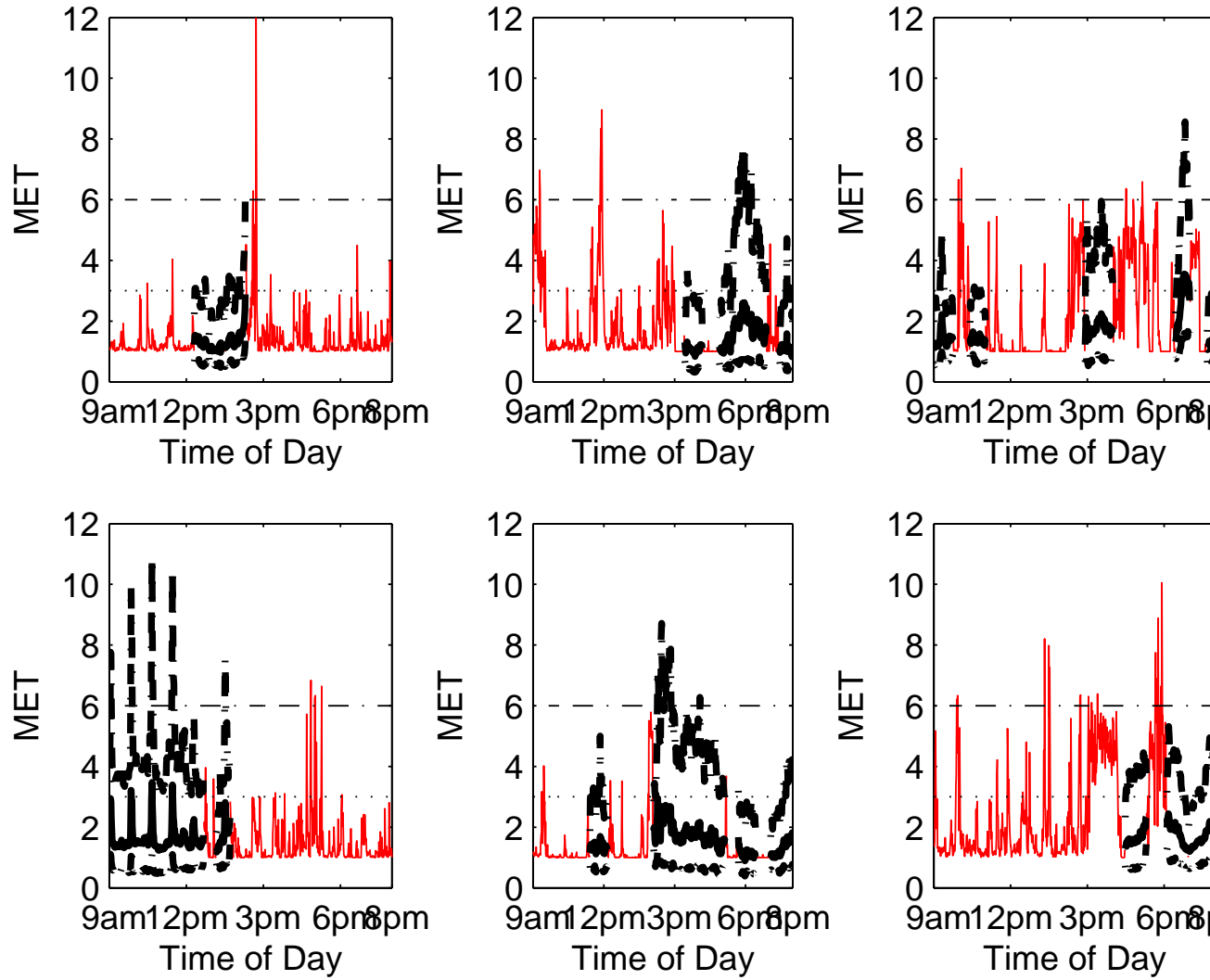


Figure 4: Imputation distributions. Some incomplete profiles, with mean and 95% pointwise bounds from the joint imputation distribution substituted for the missing regions, based on the normal approximation to the posterior predictive distribution estimated from posterior samples obtained from a Markov Chain Monte Carlo scheme applied to the complete case data.

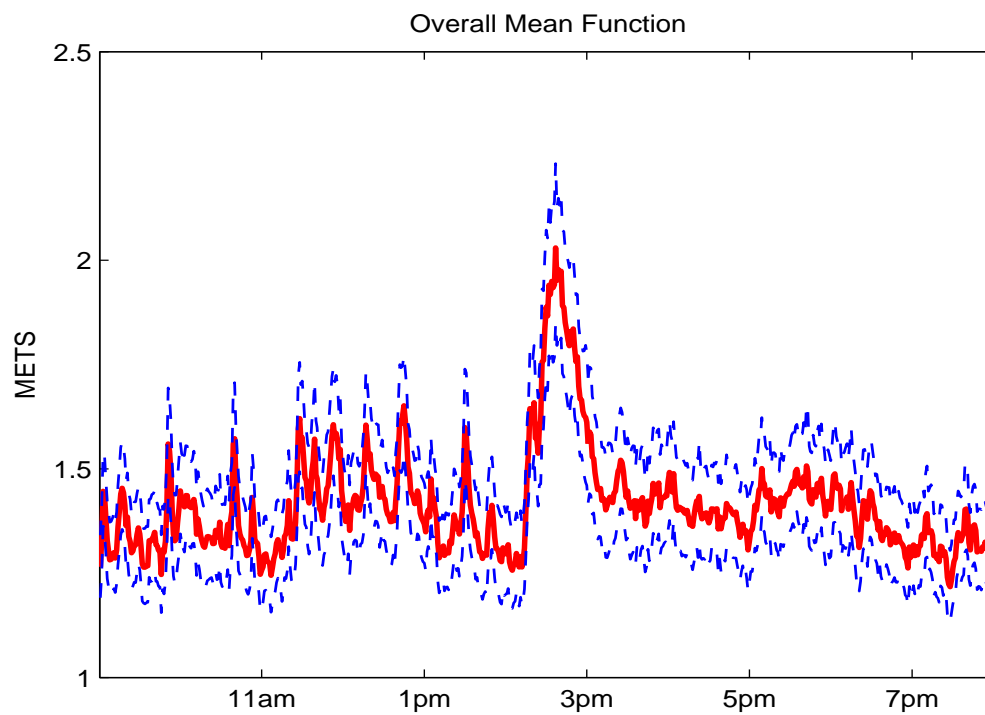


Figure 5: Overall Mean Curve. Posterior mean and 90% pointwise credible bounds for the overall mean curve, obtained by averaging equally over the schools and conditioning on the mean value in the data set for all other covariates.

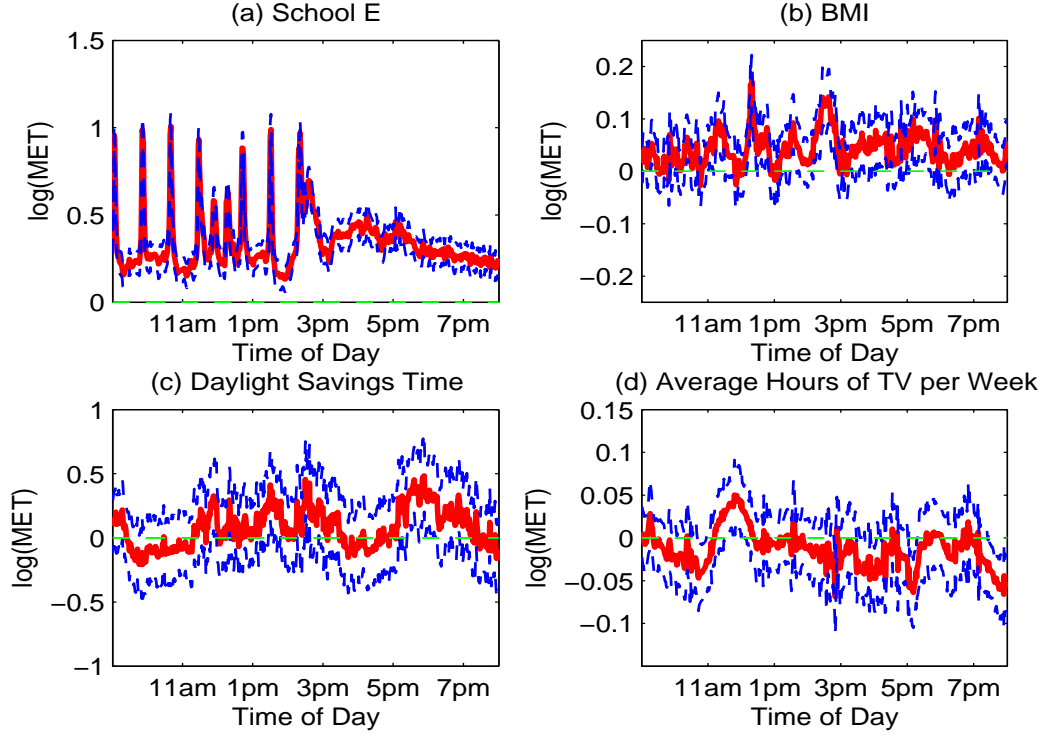


Figure 6: Fixed Effect Curves. Posterior mean curves and 90% pointwise posterior credible intervals for the fixed effects curves for (a) school E, (b) body mass index, (c) daylight savings time, and (d) average hours of television per day. The curve in (a) can be interpreted as the mean log profile on a Monday before daylight savings time for a child from school E with average BMI who is average with respect to the average number of hours of TV they watch per day. The curve in (b) is the amount added (or subtracted) to a child's mean log activity profile per unit increase (or decrease) in BMI. The curve in (c) is added to the mean log profile for any day after daylight savings time (April 6). The curve in (d) is the amount added (or subtracted) to the mean log profile for each standard deviation unit above (or below) the mean for that child with respect to their average hours of television watched per day.

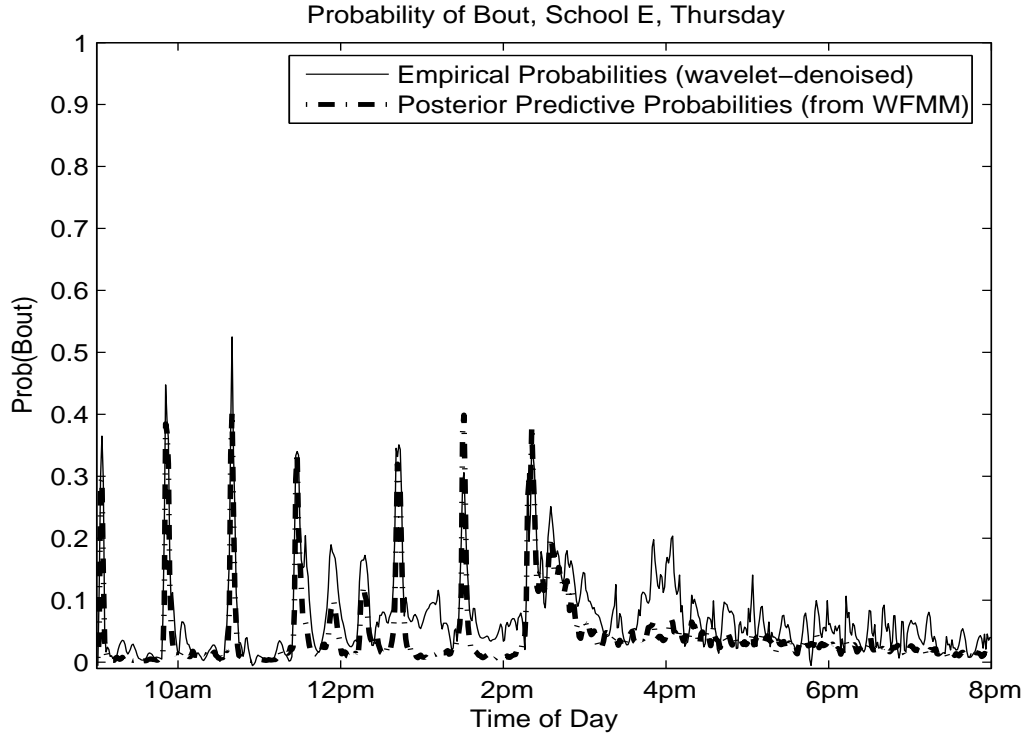


Figure 7: Posterior Predictive Probabilities of Bouts. The solid line indicates the wavelet-denoised empirical probabilities of bouts for each time point averaging over the 42 accelerometer profiles obtained on Thursdays from children enrolled at school E. The dashed-dotted line indicates the posterior predictive probability of bouts from the functional mixed model for a child enrolled at school E on Thursday, for whom the levels of all other covariates are at their mean levels.